

GNSS signal phase, TEC, and phase unwrapping errors

Charles Rino¹  | Brian Breitsch¹ | Yu Morton¹  | Dongyang Xu² | Charles Carrano³

¹ University of Colorado

² Colorado State University

³ Institute for Scientific Research,
Boston College

Correspondence

Charles Rino, University of Colorado.
Email: crino@comcast.net

Funding information

Air Force Office of Scientific Research,
Grant/Award Number: FA8650-14-D-1725.

Abstract

Precise measurements of signal phase are essential for Global Navigation Satellite System (GNSS) position estimates. However, propagation through the earth's ionosphere imposes frequency-dependent phase errors. The frequency dependence is exploited to correct phase errors proportional to total electron content (TEC) divided by frequency. Scintillation causes additional stochastic errors, which can become the largest phase error contribution. Both geometry-free (GFCs) and ionosphere-free (IFCs) frequency combinations are subject to such uncorrectable but generally small *phase scintillation* errors. A recent published study compared GPS TEC estimates derived from nominally identical L1-L2 and L1-L5 GFCs. The TEC errors establish an upper bound on uncorrelated single-frequency scintillation error contributions. The measured TEC errors were verified with phase-screen simulations. However, a known but largely overlooked phase unwrapping error affects the extraction of signal phase from phase-screen complex signal realizations. This paper demonstrates a procedure for detecting and correcting phase-unwrapping errors and discusses their ramifications.

1 | INTRODUCTION

Precise phase measurement is an integral part of GNSS signal processing. However, unlike signal intensity and delay, phase cannot be measured directly. Formally, phase is extracted from a complex product of two complex time series with nearly identical frequencies. In purely mathematical terms, phase is derived from a 2π -ambiguous nonlinear inverse tangent operation. For GNSS applications, smoothly varying phase reports are essential, whereby a considerable ongoing effort has been devoted to detecting and repairing *cycle slips* (Breitsch et al., 2020). There is a well-know algorithm that will recover unwrapped phase from a sequence of 2π ambiguous samples. The algorithm is not used directly for GNSS processing because it operates on an extended set of data samples. However, phase reconstruction is used to provide

phase *truth* for evaluating cycle-slip recovery schemes and GNSS system performance under disturbed propagation conditions.

Theoretical scintillation models are being used to generate realizations of propagation disturbances that can be mapped onto signal realizations for direct performance analysis. In the process of investigating the phase structure generated by phase-screen simulations, we found a known but largely neglected problem with the phase unwrapping operation that reconstructs the wrapped inverse tangent phase. The unwrapping operation only produces jump-free phase reconstructions when the sample differences do not exceed π radians. We demonstrate a modification of the unwrapping procedure that will detect and remove residual phase jumps. The remainder of this paper will describe a modified phase reconstruction utility that will detect and correct the phase derived from complex

signal realizations. Readers interested mainly in the phase unwrapping problem can skip to the Complex Signal Phase Extraction section.

Global Navigation System Satellite (GNSS) receivers measure signal intensity, phase, and delay as frequency-dependent time series. Irrespective of the complex modulation that defines the GNSS signals, measurements can be interpreted against the following parametric signal model, which was introduced in Rino et al. (2018):

$$I(t; f_c) = P(t)|h(t; f_c)|^2 + \dots \quad (1)$$

$$\frac{\lambda_c}{2\pi} \phi(t; f_c) = r(t) - cK \cdot TEC(t)/f_c^2 - \frac{\lambda_c}{2\pi} \phi_s(t; f_c) + \dots \quad (2)$$

$$c\tau(t; f_c) = r(t) + cK \cdot TEC(t)/f_c^2 + \frac{\lambda_c}{2\pi} \phi_s(t; f_c) + \dots \quad (3)$$

The leading term, $r(t)$ in Equations (2) and (3), represents the true propagation distance (range), f_c represents the carrier frequency, and $\lambda_c = c/f_c$ is the carrier wavelength with c as the vacuum velocity of light. The ellipses indicate omitted bias and noise contributions. Delay and phase have been scaled to pseudo-range length units. If the total electron content is measured in units of 10^{16} electrons per square meter per meter of path length, the product $cK = 40.3$. The conversion from path-integrated electron content to phase in radians is

$$\phi_{TEC}(t; f_c) = -2\pi K \cdot TEC(t)/f_c. \quad (4)$$

The following definition of the complex modulation identifies the stochastic TEC and scintillation components explicitly:

$$h(t; f_c) = |h(t; f_c)| \exp\{-i(2\pi K \cdot \Delta TEC(t)/f_c + \phi_s(t; f_c))\}. \quad (5)$$

Equation (1) in Nguyen et al. (2019) also identifies the ionospheric error terms explicitly. In their notation, $L_f = \phi(t; f_c)\lambda_c/(2\pi)$. Our TEC and scintillation terms when scaled to range units coincide respectively with I_f' and I_f^d in their notation. In textbook versions of the signal model, phase scintillation is often lumped together with other error terms.¹ The error terms include noise, interference, multipath, and system biases as enumerated in Nguyen et al. (2019). The measured signal phase also includes a 2π phase ambiguity. For this study, only the ionospheric terms will be considered.

Geometry-free combinations (GFCs) of the frequency-dependent phase follow from Equation (2) as

$$\begin{aligned} & \frac{\phi(t, f_{c_2})/f_{c_2} - \phi(t, f_{c_1})/f_{c_1}}{2\pi K(1/f_{c_1}^2 - 1/f_{c_2}^2)} \\ &= \overline{TEC}(t) + \Delta TEC(t) + \frac{\phi_s(t, f_{c_2})/f_{c_2} - \phi_s(t, f_{c_1})/f_{c_1}}{2\pi K(1/f_{c_1}^2 - 1/f_{c_2}^2)}. \end{aligned} \quad (6)$$

In the absence of scintillation, GFCs estimate the combined deterministic and stochastic TEC contributions to the signal phase. Although single-frequency phase scintillation contributions cannot be isolated, the scintillation-induced TEC errors can be isolated by subtracting nominally identical TEC estimates derived from GPS L1-L2 and L1-L5 GFCs. A study reported by Rino et al. (2019) found TEC scintillation errors to be less than one TEC unit when the S4 scintillation index at the L2 or L5 frequency was less than 0.5. This implies that for the weak-to-moderate scintillation conditions that apply to most GNSS observations, scintillation-induced TEC errors for ionospheric diagnostic measurements are negligibly small. The TEC error bounds were corroborated in Rino et al. (2019) with phase-screen simulations.

2 | PHASE-SCREEN PROPAGATION MODELS

The time series that characterize the complex modulation imparted to GNSS signals are generated by translation of the propagation paths through structured regions. A complete calculation requires knowledge of the varying positions of the source and receiver, the location and extent of the structure, the structure drift, and the direction of the magnetic field. Fortunately, a comparatively small number of parameters capture the critical dependencies on structure, propagation distance, and time-to-space translation. Propagation effects are determined by the Fresnel scale

$$\rho_F = \sqrt{r_F/k}, \quad (7)$$

where r_F is the effective propagation distance from the structured region to the receiver, and $k = 2\pi f_c/c$ is the propagation vector magnitude. Space-to-time conversion is achieved by replacing the Fresnel-scale with ρ_F/v_{veff} where v_{veff} is an effective scan velocity, which incorporates the dependence on the scan direction relative to the magnetic field direction. Representative values can be used without specifying the propagation geometry details, as described in Carrano and Rino (2016), Jiao et al. (2018),

¹ See Misra and Enge (2012), equations (5.46) and (5.47).

Xu et al. (2019), and Carrano et al. (2019). A phase-screen model that captures the signal structure is described in Rino et al. (2018).

The model is revisited here because, as will be shown in the next section, phase-screen sampling impacts phase reconstruction. The phenomenon is demonstrated with complex field realizations initiated with stochastic phase realizations. The phase structure is characterized by a spectral density function (SDF), which is the average intensity of a Fourier decomposition of the process. For a time series, the term power spectral density (PSD) usually replaces SDF, which is the more general term. A standard procedure for generating phase realizations with SDF Φ_m follows:

$$\phi_n = \sum_{m=0}^{N-1} \sqrt{\Phi_m \Delta q / (2\pi) \eta_m} \exp\{2\pi i n m / N\}. \quad (8)$$

The random variable, η_m , is a zero-mean, unit-variance, uncorrelated (white noise) process. Formally, $\langle \eta_m \eta_{m'}^* \rangle = \delta(m - m')$. Angle brackets denote ensemble averaging. With the SDF, Φ_m , specified, a complex field realization can be generated with two discrete Fourier transformation (DFT) operations as follows:

$$\psi_n = \exp\{i\phi_n\} \quad (9)$$

$$\hat{\psi}_m = \sum_{n=0}^N \psi_n \exp\{-2\pi i n m / N\} \quad (10)$$

$$\psi_n = \frac{1}{N} \sum_{m=0}^N \hat{\psi}_m \exp\{-i\mu_n^2 / 2\} \exp\{2\pi i n m / N\}, \quad (11)$$

where $\mu_m = \rho_F q_m$ is a scale free measure of the spatial wavenumber.

Carrano and Rino (2016) developed a two-dimensional scintillation theory for unbounded two-component power-law structures. Efficient algorithms are available for computing the intensity SDF, Φ_I , the scintillation index, $S4$, and the complex field SDF, Φ_ψ . Calculations are initiated by specifying the following scale-free form of the two-component phase SDF:

$$[\Phi_\phi(\mu) / \rho_F] = C_{pp} \begin{cases} \mu^{-p_1} & \text{for } \mu \leq \mu_0 \\ \mu_0^{p_2 - p_1} \mu^{-p_2} & \text{for } \mu > \mu_0 \end{cases}, \quad (12)$$

where $\mu_0 = \rho_F q_0$ and $C_{pp} = C_p \rho_F^{-p_1}$. The defining parameters are C_{pp} , p_1 , μ_0 , and p_2 . However, it was found to be more convenient to use the *universal strength parameter*

$$U = C_{pp} \begin{cases} 1 & \text{for } \mu_0 > 1 \\ \mu_0^{p_2 - p_1} & \text{for } \mu_0 \leq 1 \end{cases}, \quad (13)$$

which determines the severity of the scintillation as measured by the $S4$ index

$$S4^2 = \int_0^\infty [\Phi_I(\mu) / \rho_F] \frac{d\mu}{\pi}. \quad (14)$$

For $U < 1$, $S4 \ll 1$. As U increases, $S4$ approaches unity. As U increases further, $S4$ may exceed unity or achieve a local maximum after which $S4$ recedes to a value approaching unity from above.

The theory also provides analytic representations of the phase structure function, D , the mutual coherence function, MCF , and the complex field SDF, Φ_ψ :

$$\begin{aligned} D(\delta y) &= \langle (\phi(y) - \phi(y'))^2 \rangle / 2 \\ &= \frac{1}{\pi} \int_0^\infty \sin^2(\delta y q / 2) \Phi_\phi(q) dq \end{aligned} \quad (15)$$

$$\begin{aligned} MCF(\delta y) &= \langle \psi(y) \psi^*(y') \rangle \\ &= \exp\{-D(\delta y)\} \end{aligned} \quad (16)$$

$$\Phi_\psi(q) = \int_0^\infty MCF(\delta y) \cos(q\eta) d\delta y. \quad (17)$$

The notation δy is used to avoid confusion with the sample interval Δy . The MCF and the complex field SDF are defined by the phase screen. However, they remain invariant as the complex field propagates away from the phase screen. This well-known property of freely propagating stochastic plane-wave fields follows from the diffraction operator in Equation (11), which modifies only the phase of the propagating plane waves that comprise the field.

As discussed in Carrano and Rino (2016), the software implementation of the theory generates normalized SDFs as functions of μ . The μ range is sampled non-uniformly from μ_{\min} to μ_{\max} . For applications, a uniformly sampled μ range is generated by interpolation. Physical units are defined by the spatial extent Y and the sampling interval Δy or the temporal extent T and the sampling interval Δt . The corresponding frequency ranges are

$$q_m = m \Delta q \text{ where } \Delta q = 2\pi / Y \quad (18)$$

$$f_m = m \Delta f \text{ where } \Delta f = 1 / T. \quad (19)$$

The Fresnel scale factors ρ_F and ρ_F / v_{veff} convert the physical frequency ranges q_m and f_m to the scale-free frequency range μ_m . Hereafter, only spatial units will be used with the understanding that conversion to time and temporal frequency is achieved by replacing ρ_F with ρ_F / v_{veff} .

The components of the Fourier transform pair $MCF(\eta) \Leftrightarrow \Phi_\psi(q)$ provide guidance for sampling. If they are well-contained within the respective intervals Y and Q , both functions can be computed accurately with an N -point DFT pair with sampling $\Delta\delta\eta$ and Δq , corresponding to the Δy and Δq sampling of the complex field realizations. Furthermore, Fourier interpolation, which multiplies N by zero-extending the discrete Fourier transform accordingly, accurately represents the interpolated complex field samples. However, the intensity and phase of the complex signal are derived from nonlinear operations that impose more stringent sampling requirements. As described in the Appendix, the theoretical intensity SDF can be used to determine sampling requirements for intensity reconstruction. We have no analytic theory against which phase reconstruction can be verified, whereby we must rely on consistency checks as described in the next section.

2.1 | Complex signal phase extraction

Extracting phase from a discrete complex series, ψ_n , starts with the *wrapping* operation

$$W\{\psi_n\} = \arctan\{\text{imag}\{\psi_n\}, \text{real}\{\psi_n\}\} = \phi_n + 2\pi k_1. \quad (20)$$

If there are phase changes such that $|\phi_{n-1} - \phi_n| \geq \pi$, the transitions cannot be unambiguously resolved without further analysis. However, if $|\phi_{n-1} - \phi_n| < \pi$, perfect reconstruction can be achieved with a well-known *unwrapping* algorithm. We will refer to any single-step phase change greater than one cycle (2π radians) as a *phase jump* to distinguish it from a cycle slip as defined in Nguyen et al. (2019). Following the development of Itoh's algorithm as reviewed in chapter 1.3.1 of Ghiglia and Pritt (1998), we apply the wrapping operation to the differences of the wrapped phase. The result is

$$W\{\Delta W\{\psi_n\}\} = \Delta\phi_n + 2\pi(\Delta k_1 - k_2), \quad (21)$$

where k_2 is the unwrapping error for the difference. If there are no phase jumps, $\Delta k_1 - k_2 = 0$. A phase-jump-free phase sequence is recovered by summing the unwrapped difference $W\{\Delta W\{\psi_n\}\} = \Delta\phi_n$. Although perfect reconstruction can be achieved if there are no phase jumps *at the current sampling interval*, the phase associated with critically sampled complex fields may not satisfy the jump-free criteria.

To introduce some notation, let $N \times n_{int}$ represent the size of a zero-extended DFT. An inverse DFT applied to the zero-extended original DFT will repeat the original samples at intervals n_{int} followed by $n_{int} - 1$ interpolated

samples. Thus, $n_{int} = 1$ implies no interpolation. Contributions at the Nyquist frequency must be zero, which imposes a strict periodicity constraint. However, phase-screen realizations automatically satisfy this constraint. To test the unwrapping operation at interpolation level $n_{int}N$, we generate an interpolated sequence $\bar{\psi}_n$ with $(n_{int} + 1)N$ samples and apply the following test to see if the common samples have changed:

$$\phi_n == \text{unwrap}\{\arctan\{\text{real}\{\bar{\psi}_{2n-1}\}, \text{imag}\{\bar{\psi}_{2n-1}\}\}\}. \quad (22)$$

The double equal sign operation generates ones where there is equality and zeros otherwise. If there are no disparities, the phase has been correctly unwrapped at level n_{int} . The operation can be repeated with n_{int} replaced by $n_{int} + 1$ until Equation (22) is satisfied. With noise-free complex samples, the interpolation limit is determined by numerical resolution.

To illustrate unwrapping error detection and correction, a 200-km stochastic phase realization was generated with 8,192 samples, whereby the initiating phase is known. The turbulent strength parameter C_{pp} was increased until unwrapping errors were observed when the unit-intensity complex signal phase was unwrapped. The upper left frame of Figure 1 shows the phase realization (blue) with the unwrapped phase overlaid in (red). The disparity between the initiating phase and the unwrapped phase is a small fraction of the total phase. However, the absolute errors shown in the lower frame are significant. The nominal phase difference computed from Equation (21) is shown in the lower left frame (blue). The right frame shows the same results with $n_{int} = 2$, which reproduces the original phase sequence without error. For a critically sampled complex field, which is intrinsically smooth at the finest sampling level, interpolation can be increased until perfect reconstruction of the original phase samples has been achieved.

3 | UNWRAPPING ERROR RAMIFICATIONS

We showed in the previous section that the phase of a complex series may be inadequately sampled for conventional phase unwrapping even if the complex signal itself is critically sampled. The complex signal amplitude has no direct impact on phase unwrapping. However, strong amplitude scintillation is associated with highly structured phase scintillation, which is more prone to unwrapping errors. Phase-screen realizations were generated as described in the previous section. The upper frame of Figure 2

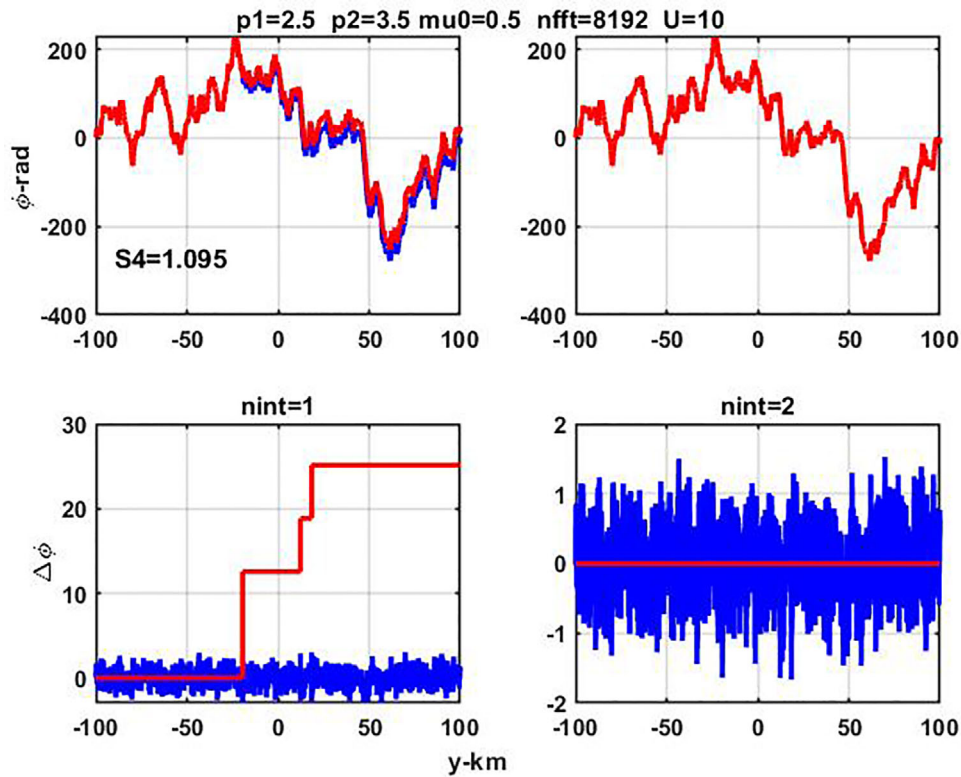


FIGURE 1 Upper left frame shows initiating phase (blue) and unwrapped phase (red). The S4 L1 index at 350 km is indicated for reference. The lower left frame shows the unwrapped phase (blue) and the error (red). The right-hand frame shows the same displays with unwrapping phase correction [Color figure can be viewed in the online issue, which is available at wileyonlinelibrary.com and www.ion.org]

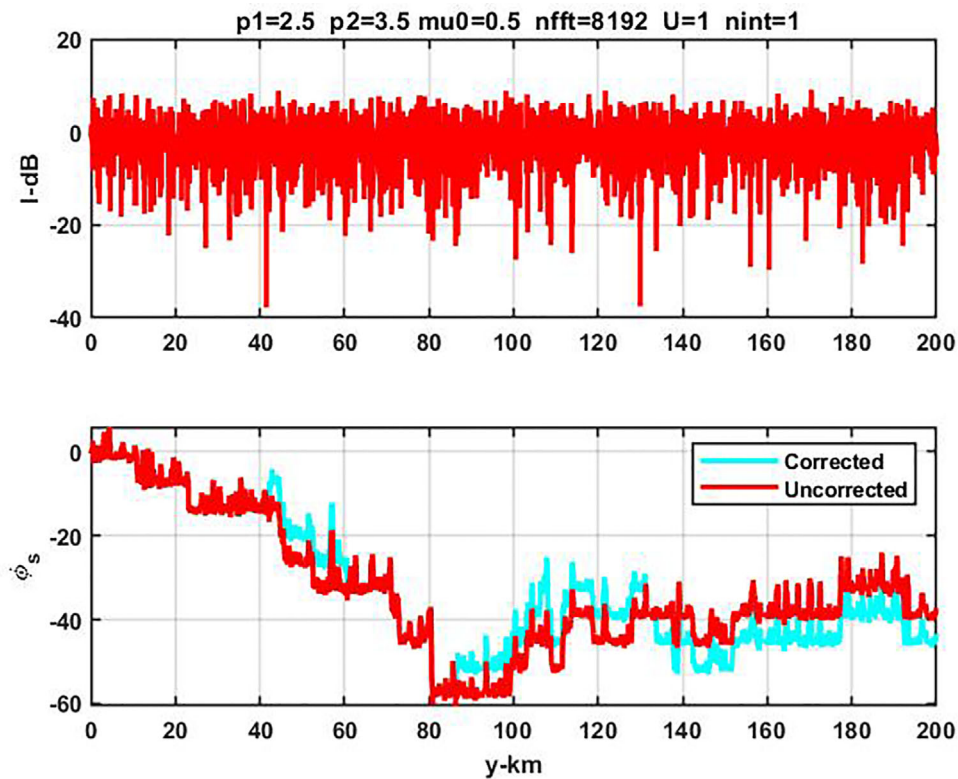


FIGURE 2 Upper frame shows the interpolated intensity realization (red). Lower frame shows initial (red) and corrected (cyan) phase. The starting distance is arbitrary [Color figure can be viewed in the online issue, which is available at wileyonlinelibrary.com and www.ion.org]

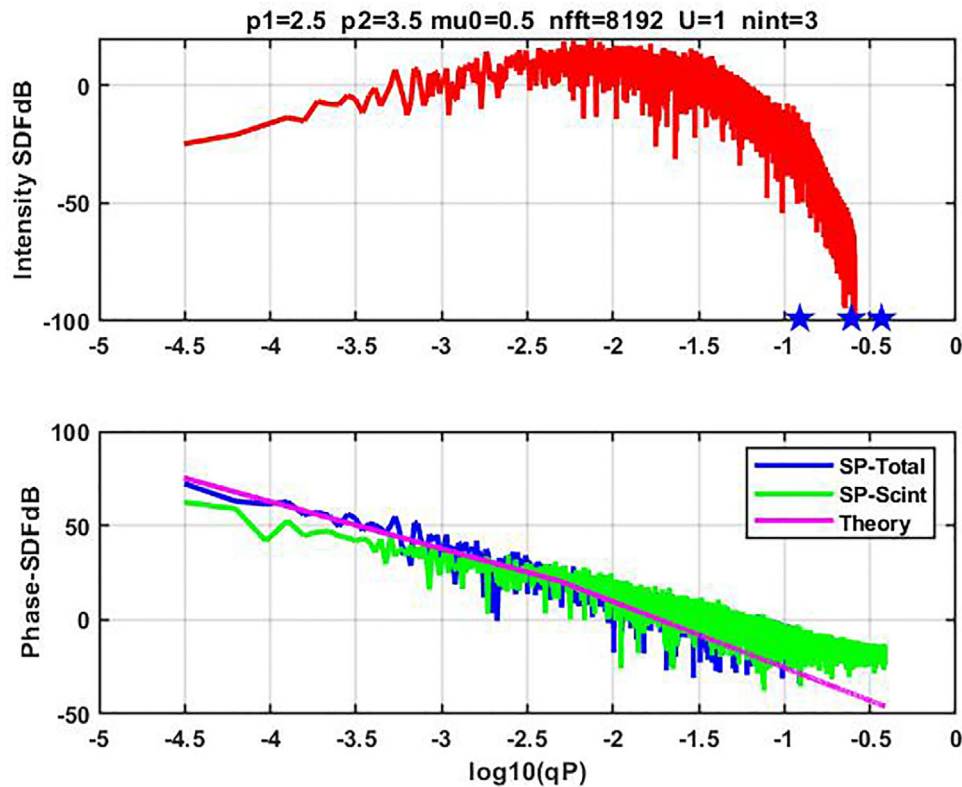
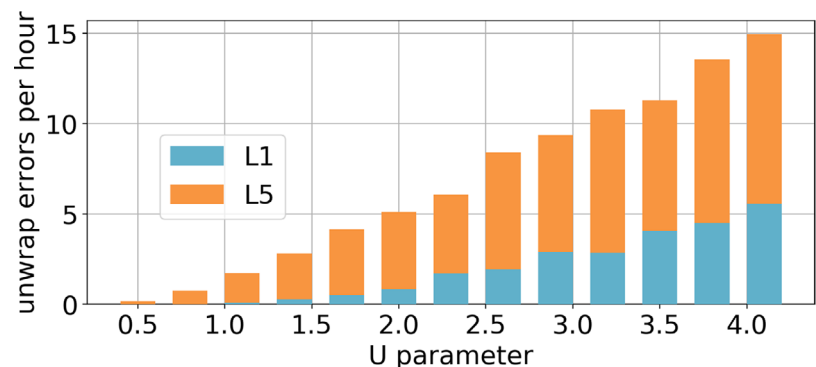


FIGURE 3 Upper frame shows intensity SDF for $U = 1$ realization. Lower frame shows the phase SDF (blue), the scintillation SDF (red), and the theoretical SDF for the initiating stochastic phase (green) [Color figure can be viewed in the online issue, which is available at wileyonlinelibrary.com and www.ion.org]

FIGURE 4 Phase $L1$ and $L5$ unwrapping errors versus U at $L1$ [Color figure can be viewed in the online issue, which is available at wileyonlinelibrary.com and www.ion.org]



shows the $U = 1$ observation-plane intensity realization derived from the phase realization shown in Figure 1. The intensity is sampled at the minimum sampling that supports error-free phase unwrapping of the complex signal phase, namely $3N = 24386$. The lower frame shows the uncorrected phase (red) and the corrected phase (cyan).

The upper frame of Figure 3 shows the SDF of the interpolated intensity realization. The pentagrams mark the Nyquist frequencies for $n_{int} = 1, 2,$ and 3 sampling. The intensity content beyond the complex signal Nyquist

frequency occupies only the range from the Nyquist frequency to twice the Nyquist frequency. However, that extension is not an extrapolation of the theoretic SDF. Increasing the sampling of the initiating phase screen is necessary to increase the intensity resolution. The lower frame in Figure 3 shows the SDF of the signal phase (blue) with the scintillation SDF overlaid (red).

Figure 4 shows the occurrence of unwrapping errors plotted against U at the $L1$ frequency. The lower $L2$ and $L5$ frequencies correspond to higher U values. The occurrence of unwrapping errors is confined to stronger

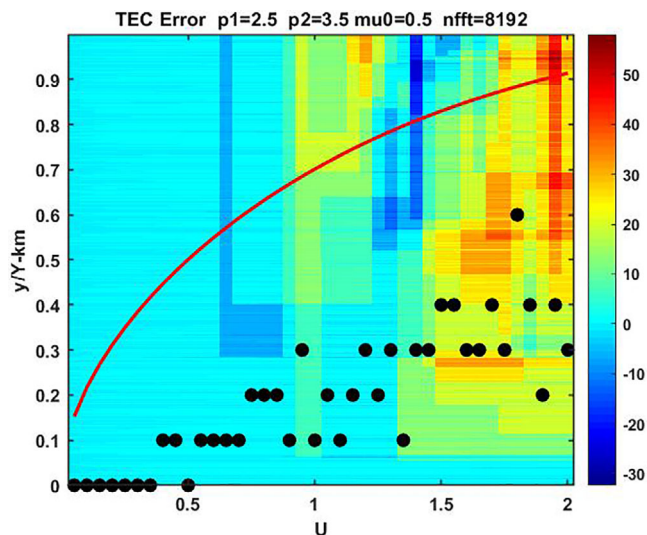


FIGURE 5 TEC errors versus U derived from complex field realizations corresponding to L1 and L2 realizations at 350 km. The ordinate is scaled to the maximum distance to allow superposition of the S4 index in red. The black dots indicate the level of iteration required for error-free unwrapping [Color figure can be viewed in the online issue, which is available at wileyonlinelibrary.com and www.ion.org]

scintillation conditions. Fewer than six iterations with typically no more than three iterations generated error-free phase unwrapping. Interpolation does not change the common intensity samples, but as noted above, increasing the spectral range coincident with the theory requires recalculation of the propagation effects.

To demonstrate the effects of phase unwrapping errors, Figure 5 shows a recalculation of the TEC errors shown in Figure 5 from Rino et al. (2019) with unwrapping error detection and correction. The distance scale has been normalized to generate a zero-to-one scale for the S4 index at L1, which is overlaid in red. The black dots, which are computed as $(n_{int} - 1)/10$ for display, show the interpolation required to correct unwrapping errors. The unwrapping error occurrence is consistent with the results shown in Figure 4. The first seven realizations required no interpolation. In effect, the occurrence of unwrapping errors coincides with significant TEC errors. The main conclusion, namely that significant TEC errors are negligibly small under weak to moderate scintillation conditions, is unchanged.

4 | SUMMARY AND CONCLUSIONS

We showed that a standard procedure used to extract a phase from a complex series may not generate a phase series free from phase jumps, as illustrated in Figure 1.

These residual phase jumps are caused by sampled-dependent phase changes greater than π radians. A critically sampled complex series supports interpolation that will ultimately eliminate phase changes greater than π radians. We demonstrated a successive interpolation procedure that detects and removes any residual phase jumps. Functionally, critical sampling means that the phase associated with the complex field has no discontinuities. This constraint does not preclude the very large phase changes associated with the so-called canonical scintillation deep fades. Noise-free phase-screen simulations generate very large phase changes, but when properly sampled, the phase variations are resolved (Carrano et al., 2013).

We showed also that the occurrence of phase jumps in phase-screen realizations is confined to large propagation disturbances. Revisiting simulations of TEC scintillation errors identified with three-frequency geometry-free GPS measurements (Rino et al., 2019), we found that phase jumps occurred under the same conditions that produced large scintillation-induced TEC errors. There was no impact on the critical finding, namely that scintillation-induced TEC errors are negligible for diagnostic measurements under weak to moderate scintillation conditions. In the same way, recent performance evaluations reported by Xu et al. (2019) are largely unaffected by uncorrected phase jumps because they are statistically similar to large but resolved phase changes. For future studies that use complex field simulations as truth, corrected phase extraction should be used.

Diagnostic phase measurements are most often generated by signal-processing procedures that track incremental phase or frequency changes. Cycle slips, which are highly processor and sample dependent, are attributed to the processor errors. The study by Nguyen et al. (2019) associated cycle slips with phase scintillation as distinct from the more smoothly varying correctable TEC contributions. Furthermore, signal processing operations are acutely sensitive to noise, which has not been considered. In a recent paper by Breitsch et al. (2020), a systematic procedure for identifying rapid local phase changes as cycle slips and demonstrating their dependence on noise and scintillation intensity was demonstrated. Simulated and measured cycle slips showed remarkably similar characteristics. Comparing corrected unwrapped phase sequences and measured phase sequences should provide insights into both the diffraction processes that generate rapid phase changes and signal processing operations that encounter the changes.

An updated MatLab scintillation model with examples of unwrapping error correction and sample adequacy checks can be downloaded from <https://github.com/cu-sense-lab/gnss-scintillation-simulator>

ACKNOWLEDGMENTS

The results in the paper can be reconstructed with the MatLab software provided. The reported research was supported in part by the Air Force Office of Scientific Research grant FA8650-14-D-1725.

ORCID

Charles Rino  <https://orcid.org/0000-0003-2560-0478>

Yu Morton  <https://orcid.org/0000-0001-9173-2888>

REFERENCES

- Breitsch, B., Morton, Y. T., Xu, D., & Yang, R. (2020, January). Ionosphere scintillation-induced phase transitions in triple-frequency GPS measurements. *Proceedings of the 2020 International Technical Meeting of The Institute of Navigation*, San Diego, CA, 912–919. <https://doi.org/10.33012/2020.17186>
- Carrano, C. S., Groves, K. M., McNeil, W. J., & Doherty, P. H. (2013, January). Direct measurement of the residual in the ionosphere-free linear combination during scintillation. *Proceedings of the 2013 International Technical Meeting of The Institute of Navigation*, San Diego, CA, 585–596.
- Carrano, C. S., Groves, K. M., & Rino, C. L. (2019). On the relationship between the rate of change of total electron content index (ROTI), irregularity strength (CkL) and the scintillation index (s4). *Journal of Geophysical Research: Space Physics*, 124(3), 2099–2112. <https://doi.org/10.1029/2018JA026353>
- Carrano, C., & Rino, C. (2016). A theory of scintillation for two-component power law irregularity spectra: Overview and numerical results. *Radio Science*, 51, 789–813. <https://doi.org/10.1002/2015RS005903>
- Chiglia, D. C., & Pritt, M. D. (1998). *Two-dimensional phase unwrapping theory, algorithms, and software*. John Wiley & Sons, Inc.
- Jiao, Y., Xu, D., Rino, C., Morton, Y., & Carrano, C. (2018). A multi-frequency GPS signal strong equatorial ionospheric scintillation simulator: Algorithm performance and characterization. *IEEE Transactions on Aerospace Electronic Systems*, 54(4), 1947–1965. <https://doi.org/10.1109/TAES.2018.2805232>
- Misra, P., & Enge, P. (2012). *Global positioning system signals, measurements, and performance*. Ganga-Jamuna Press.
- Nguyen, V. K., Rovira-Garcia, A., Juan, J. M., Sanz, J., González-Casado, G., La, T. V., & Ta, T. H. (2019). Measuring phase scintillation at different frequencies with conventional GNSS receivers operating at 1 Hz. *Journal of Geodesy*, 93, 1985–2001. <https://doi.org/10.1007/s00190-019-01297-z>
- Rino, C., Briestch, B., Morton, Y., Jiao, Y., Xu, D., & Carrano, C. (2018). A compact multifrequency GNSS scintillation model. *NAVIGATION*, 65(4), 563–569. <https://doi.org/10.1002/navi.263>
- Rino, C., Morton, Y., Briestch, B., & Carrano, C. (2019). Stochastic TEC structure characterization. *JGR Space Physics*, 124(12), 10571–10579. <https://doi.org/10.1029/2019JA026958>
- Xu, D., Morton, Y., & Yang, R. (2019). A comparative performance analysis of advanced GNSS carrier tracking algorithms during strong equatorial ionospheric scintillation. *IEEE Transactions on Aerospace Electronic Systems*. <https://doi.org/10.1109/TAES.2020.3011999>

How to cite this article: Rino C, Breitsch B, Morton Y, Xu D, Carrano C. GNSS signal phase, TEC, and phase unwrapping errors. *NAVIGATION*. 2020;67:865–873. <https://doi.org/10.1002/navi.396>

APPENDIX

The algorithmic encapsulation of the two-dimensional phase-screen theory in Carrano and Rino (2016) generates normalized SDFs as functions of $\mu = \rho_F q$. The μ range is sampled non-uniformly from μ_{\min} to μ_{\max} . For applications, the non-uniformly sampled range must be interpolated to

$$n\Delta\mu = \rho_F n\Delta q \text{ for } n = 1, 2, \dots, N. \quad (\text{A1})$$

This involves a choice of ρ_F , Δq , and N . If estimates \hat{S}_4 and $\hat{\Phi}_1(n)$ are available, model parameters can be adjusted to match the theory. Figure A1 shows the non-uniformly sampled model output for the defining parameters in the title with a uniformly sampled overlay.

The red curve might represent the best fit range for the measured SDF and S4. However, for modeling purposes, we often have a specified N and Δq for which a range of scintillation strengths are of interest. One can then ask what range of ρ_F values are appropriate for realizations defined by fixed structure parameters. The effect of changing ρ_F with all the other parameters fixed is to slide the red curve in Figure A1 along the blue curve. It is intuitively

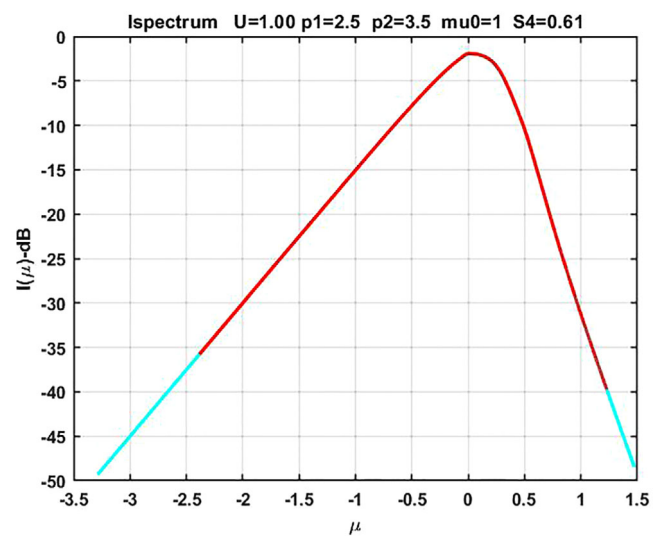


FIGURE A1 Model calculations of Intensity SDF versus μ . Blue curve is non-uniformly sampled model output. Red curve is a uniformly sampled subset for a specified ρ_F [Color figure can be viewed in the online issue, which is available at wileyonlinelibrary.com and www.ion.org]

clear that a good choice for ρ_F captures the largest values of the intensity SDF. This can be formalized by choosing ρ_F to minimize the difference between the sampled estimate of

$$\hat{S}_4^2 = \sum_{n=1}^N [\Phi_I(\rho_F q_n) / \rho_F] \frac{\rho_F \Delta q}{\pi} \quad (\text{A2})$$

and the theoretical value. An algorithm for performing this computation is included in the revised phase-screen model. The red curve shown in Figure A1 was plotted using the algorithm calculation of ρ_F . The choice of the Fresnel scale is constrained by the phase-screen sampling. For example, the optimum sample range for smaller and smaller values of N will ultimately generate a realization too small to resolve the contributing structure.